Biochimica et Biophysica Acta 1830 (2013) 5095–5103

Contents lists available at ScienceDirect

Biochimica et Biophysica Acta

journal homepage: www.elsevier.com/locate/bbagen

When size does matter: organelle size influences the properties of transport mediated by molecular motors

María Cecilia De Rossi [a], Luciana Bruno [b], Alejandro Wolosiuk [c], Marcelo A Despósito [b], Valeria Levi [a,*]

[a] Departamento de Química Biológica, IQUIBICEN–CONICET, Facultad de Ciencias Exactas y Naturales, Universidad de Buenos Aires, Ciudad Universitaria, CP 1428 Ciudad de Buenos Aires, Argentina
[b] Departamento de Física, Facultad de Ciencias Exactas y Naturales, Universidad de Buenos Aires, Ciudad Universitaria, CP 1428 Ciudad de Buenos Aires, Argentina
[c] Gerencia de Química — Centro Atómico Constituyentes — Comisión Nacional de Energía Atómica, Av. Gral. Paz 1499, 1650 San Martín, Buenos Aires, Argentina

ARTICLE INFO

Article history:
Received 8 February 2013
Received in revised form 7 May 2013
Accepted 29 June 2013
Available online 16 July 2013

Keywords:
Single particle tracking
Molecular motors
Xenopus laevis melanophores
Intracellular transport
Organelle trafficking

ABSTRACT

Background: Organelle transport is driven by the action of molecular motors. In this work, we studied the dynamics of organelles of different sizes with the aim of understanding the complex relation between organelle motion and microenvironment.
Methods: We used single particle tracking to obtain trajectories of melanosomes (pigmented organelles in *Xenopus laevis* melanophores). In response to certain hormones, melanosomes disperse in the cytoplasm or aggregate in the perinuclear region by the combined action of microtubule and actin motors.
Results and conclusions: Melanosome trajectories followed an anomalous diffusion model in which the anomalous diffusion exponent (α) provided information regarding the trajectories' topography and thus of the processes causing it. During aggregation, the directionality of big organelles was higher than that of small organelles and did not depend on the presence of either actin or intermediate filaments (IF). Depolymerization of IF significantly reduced α values of small organelles during aggregation but slightly affect their directionality during dispersion.
General significance: Our results could be interpreted considering that the number of copies of active motors increases with organelle size. Transport of big organelles was not influenced by actin or IF during aggregation showing that these organelles are moved processively by the collective action of dynein motors. Also, we found that intermediate filaments enhance the directionality of small organelles suggesting that this network keeps organelles close to the tracks allowing their efficient reattachment. The higher directionality of small organelles during dispersion could be explained considering the better performance of kinesin-2 vs. dynein at the single molecule level.

1. Introduction

Molecular motors transport a wide variety of cellular components positioning them in the cytoplasm with high spatial–temporal precision. These proteins bind to specific cargoes and step along cytoskeletal filaments (i.e., microtubules or actin filaments) using energy provided by ATP hydrolysis. Biophysical properties of molecular motors have been extensively studied by single molecule/particle techniques which provided extremely valuable information in in vitro systems [1] and in living cells [2–5].

Organelle transport is driven by 3 families of motors: dynein and kinesin, which transport cargoes toward the minus and plus ends of microtubules, respectively, and myosin, responsible for the transport along actin filaments (reviewed in [6,7]). Although these motors allow motion of micrometer-sized organelles through the cytoplasm, we still do not completely understand how organelles move in the complex cellular environment in which other active and passive forces seem to play a very important role. In this context, Kulic et al. [8] studied the motion of peroxisomes along microtubule tracks and demonstrated that the movement of microtubule filaments also drives the motion of organelles. Similarly, Semenova et al. [9] proposed that the dynamics of actin filaments is essential for myosin-based transport. These studies clearly showed that the cytoskeleton cannot be only considered as static tracks.

Despite the observation that intermediate filaments are not directly involved in transport driven by molecular motors, several works showed that this network greatly affects organelle motion. Kural et al. [10] showed that disruption of the intermediate filament network in melanophore cells results in faster transport of pigmented granules along microtubules and shorter duration of the steps of the myosin V motor during melanosome transport. These authors also suggested that intermediate filaments physically hinder melanosomes by increasing

Abbreviations: IF, intermediate filaments; MSD, mean square displacement; OR, optical radius; α, anomalous diffusion exponent; FE-SEM, field emission-scanning electron microscopy; DLS, dynamic light scattering

* Corresponding author at: Departamento de Química Biológica, IQUIBICEN-CONICET, Facultad de Ciencias Exactas y Naturales, Universidad de Buenos Aires, Ciudad Universitaria, CP 1428 Ciudad de Buenos Aires, Argentina. Tel./fax: +54 11 4576 3300x205.
E-mail address: vlevi12@gmail.com (V. Levi).

0304-4165/$ – see front matter © 2013 Elsevier B.V. All rights reserved.
http://dx.doi.org/10.1016/j.bbagen.2013.06.043

the viscous drag. More recently, Chang et al. [11] showed that vimentin filaments form cage-like structures surrounding single or small clusters of melanosomes. This last study revealed that the number of moving organelles and their speed as well as their processivity increase significantly when the intermediate filaments network was disrupted. Since purified melanosomes contain a substantial amount of the intermediate filament protein vimentin, these authors suggest that melanosomes bind intermediate filaments.

Other cellular cargoes such as mitochondria are also slowed down by the intermediate filament network [12]. However the role of this cytoskeletal network on cargo mobility cannot be generalized to every cellular system. In this sense, Potokar et al. [13] explored the dynamics of single vesicles labeled with fluorescent atrial natriuretic peptides in rat astrocytes and observed that the fraction of vesicles presenting directional motion decreases in the absence of intermediate filaments.

Although, previous studies described some effects of the cellular environments on organelle transport, the low temporal resolution of those studies does not allow getting precise information about the local motion mechanisms of organelles.

Xenopus laevis melanophores are one of the most widely used cellular systems for the study of intracellular transport [14]. These cells have organelles called melanosomes, which contain the black pigment melanin and thus they can be easily observed using brightfield microscopy. Melanosomes distribute in cells in two configurations: either aggregated within the perinuclear region or homogeneously dispersed through the cytoplasm. Transport of pigment organelles during aggregation and dispersion is regulated by signaling mechanisms initiated by the binding of specific hormones to cell surface receptors, which results in the modulation of cAMP concentrations [15,16]. Organelles are transported along microtubules by the action of cytoplasmic dynein [17] and kinesin-2 [18] while myosin V is responsible for actin dependent transport [19].

In this work we used a fast and precise single particle tracking method to follow the motion of individual melanosomes in the cell cytoplasm of *X. laevis* melanophores and analyzed their trajectories to obtain information regarding the relation between organelle dynamics and local microenvironments during both the aggregation and dispersion processes. We found that small organelles, which are supposed to experience a smaller drag force, present more tortuous trajectories and found that the actin and intermediate filament networks play important roles in this behavior.

2. Materials and methods

2.1. Cell culture and sample preparation for imaging

Immortalized *X. laevis* melanophores were cultured as described in [20]. In order to track the movement of individual organelles, the number of melanosomes in cells was reduced by treatment with phenylthiourea [21]. For microscopy measurements, cells were grown for 2 days on 25-mm round coverslips placed into 35-mm plates in 2.0 ml of complete medium. Before observation, the coverslips were washed in a serum-free 70% L-15 medium (Sigma-Aldrich) and mounted in a custom-made chamber specially designed for the microscope. The cells were stimulated for aggregation or dispersion with 10 nM melatonin or 100 nM MSH, respectively. Actin depolimerization was achieved by incubation of the cells with 10 mM latrunculin B (Sigma-Aldrich) for 30 min before hormonal stimulation. Samples were observed during 15 min after stimulation.

2.2. Plasmids and tranfection

Cells grown on coverslips were transfected using Lipofectamine 2000 (Invitrogen) following the vendor instructions and observed 24 h after transfection. Two different plasmids were used: a GFP-tagged full-length *Xenopus* vimentin, which co-assembles with endogenous vimentin, and the dominant-negative construct containing the head and alpha-helical domain 1A of vimentin [GFP-vim(1-138)] that disrupt the endogenous vimentin filament network [11]. Both plasmids were a kind gift from Dr. Vladimir I Gelfand (Northwestern University, Chicago, IL).

2.3. Melanosome purification and scanning electron microscopy measurements

Melanosomes were purified and fixed onto a coverslip as described in [20,22]. In order to precisely locate every observed melanosome, SEM Au grids 400 mesh (Electron Microscopy Science, USA) were carefully glued at their ends to the coverslip and subsequently observed in the optical microscopy used for tracking measurement. Samples were then processed to be observed by field emission-scanning electron microscopy (FE-SEM). FE-SEM images were taken with a Zeiss Leo 982 Gemini microscope in the secondary-electron mode using an in-lens detector.

2.4. Nanoparticle synthesis and characterization

Gold nanoparticles were synthesized following the citrate method based in Turkevich's work [23]. Dynamic light scattering (DLS) measurements of Au nanoparticles dispersed in water showed particles with 22 nm hydrodynamic diameter with a PI = 0.20 (polydispersity index). DLS measurements were carried out in a Brookhaven BI-200 SM goniometer assembled with an avalanche photodiode detector and a He–Ne laser (wavelength = 637 nm).

2.5. Confocal microscopy

Confocal images were acquired in a FV1000 Olympus confocal microscope (Olympus Inc., Japan). EGFP fusion proteins were observed using a multi-line Ar laser tuned at 488 nm (average power at the sample, 700 nW) as excitation source. The laser light was reflected by a dichroic mirror (DM405/488) and focused through an Olympus UPlanSApo 60× oil immersion objective (NA = 1.35) onto the sample. The fluorescence was collected by the same objective, passed through the pinhole, reflected on a diffraction grating, and passed through a slit set to transmit in the range 500–600 nm. Fluorescence was detected by a photomultiplier set in the photon-counting detection mode. The pixel size was 131 nm.

Confocal imaging of C-Laurdan labeled cells was performed as described before [24] using a solid diode laser at 405 nm as an excitation source (average power at the sample, 2 μW). The laser light was reflected by a dichroic mirror (DM405/473) and focused onto the sample through the objective. Fluorescence of C-laurdan was collected by the objective, passed through the pinhole and split with a dichroic mirror into 2 independent spectral detectors set to simultaneously collect fluorescence in the range 415-455 nm and 490–530 nm (channels 1 and 2, respectively).

2.6. Tracking experiments

Single particle tracking experiments were carried out in a FV1000 Olympus confocal microscope adapted for SPT using a 40× or a 60× oil-immersion objectives (numerical aperture: 1.30 and 1.35, respectively). A high-speed electron-multiplying CCD camera (Cascade 128+, Photometrics, Tucson, AZ) was attached to the video port of the microscope for imaging the cells. Movies (2000 frames) were registered at a speed of 333 frames/s except where indicated. The accuracy on melanosome position determination was assessed by tracking melanosomes in a fixed sample and was found to be in the range 4–7 nm.

2.7. Trajectory analysis

Trajectories of melanosomes were recovered from the movies using the pattern-recognition algorithm described in [2].

The mean square displacement (MSD) was calculated from each trajectory as follows,

$$MSD(\tau) = \langle (x(t) - x(t+\tau))^2 + (y(t) - y(t+\tau))^2 \rangle, \quad (1)$$

where x and y are the coordinates of the particle, t and τ are the absolute and lag times, respectively and the brackets represents the time average. This calculation was done for τ < 10% of the total time of the trajectory [25].

The MSD data was fitted with an anomalous diffusion model similar to that proposed in our previous work [3],

$$MSD(\tau) = MSD_o + A_1 \left(\frac{\tau}{\tau_o}\right)^{\alpha}, \quad (2)$$

where τ_o is a reference value arbitrarily set to 1 s, A_1 is a constant depending on the motion properties of the particle and MSD_o is the residual MSD.

2.8. Statistical analysis

Wilcoxon ranksum test was used to compare the distributions of α values obtained for the different treatments. Analyses were performed using a *ranksum* test in MATLAB (The Mathworks, Natick, MA) and are detailed in the Supplementary materials section.

3. Results

3.1. Melanosome size determination

Single melanosomes can be considered spherical in our imaging conditions as assessed by the intensity distribution of images of the organelles (Fig. 1C). To determine the radius of melanosomes in these optical images, the intensity profile of each organelle was fitted with the sum of 3 gaussian functions:

$$I(x) = B + \sum_{i=1}^{3} A e^{-\frac{(x-xi)^2}{2\sigma^2}}, \quad (3)$$

where B is the background intensity.

The optical radius (r) of the particle was then calculated as:

$$r = \frac{|x_3 - x_1|}{2} + 2\sigma, \quad (4)$$

where x_1 and x_3 are the centers of the gaussians that are farthest from each other.

It is well known that the resolution in optical microscopy is limited by the diffraction phenomena [26]; as a consequence of diffraction, the radius determined in an optical image for micrometer-sized particles such as melanosomes is an overestimation of the real radius of the particle. In order to explore how our microscope affects the image of melanosomes, we purified these pigmented organelles and fixed them onto coverslips following the procedure described in Materials and methods. We observed the same organelles with the optical microscope used for tracking experiments and with a scanning electron microscope that provides images of the organelles with a resolution of ~5 nm (Fig. 1B–C). Since SEM images of melanosomes showed irregular borders, the radius of every particle observed by SEM was determined as the average distance between the center of the particles and different points on its perimeter. To complete this description, we also measured the optical radius of synthetic nanoparticles whose sizes were below the diffraction limit.

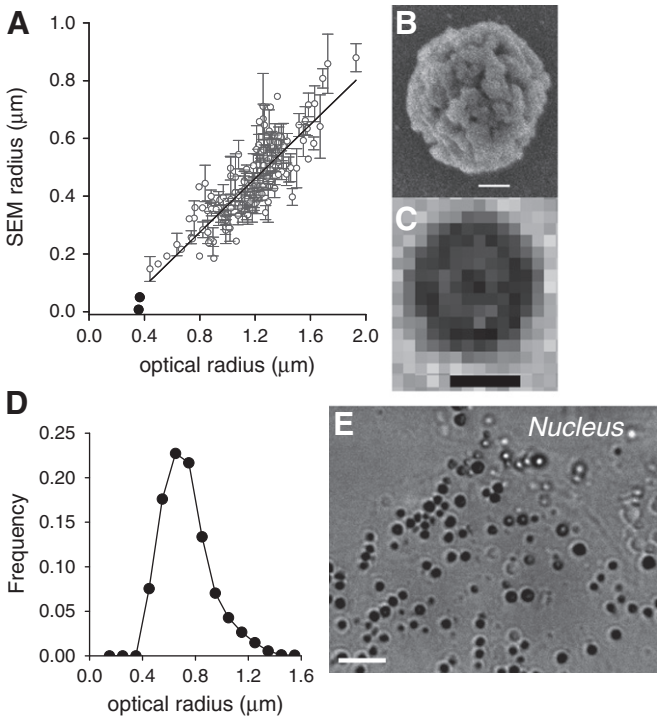

Fig. 1. Determination of melanosome sizes. (A) Dependence of the optical radius of melanosomes (O) on the radius obtained by field-emission scanning electron microscopy (FE-SEM). The plot also includes the results obtained for the optical radius of carboxylate-modified microspheres (Invitrogen) and gold nanoparticles (●). The radii of these particles were 50 nm and 11 nm, respectively. The error bars corresponds to the standard deviation on the determination of the FE-SEM radius. (B–C) Images of a melanosome obtained by FE-SEM (B) and optical microscopy (C). Scale bar: 200 nm and 1 μm, respectively. (D) Distribution of melanosomes optical radius in *Xenopus laevis* melanophores, the histogram includes data from 2700 organelles. (E) Representative image of a melanophore cell showing the distribution of melanosomes. Scale bar: 5 μm.

Fig. 1A shows that the optical radius (OR) follows a linear relation with the SEM radius in the range 500–1600 nm, importantly, Fig. 1D shows that the distribution of the melanosome optical radius in cells overlaps with this range. In the following sections we analyzed the transport properties of organelles whose radius was within this range because this guarantees that the optical radius is proportional to the size of the particle.

Since organelles in cells can move in the optical axis direction, we also tested the effect of defocusing on the optical radius determination. With this aim, we measured the OR of melanosomes in fixed cells for different z-positions of the microscope objective. On the other hand, we labeled melanophore cells with C-laurdan, a fluorescent probe used to study biological membranes [24], and recorded 3D images of the cells in a confocal microscope (see Materials and methods). We verified that the thickness of the cells in regions far from the nucleus is about ~3 μm (not shown). It is important to mention that the tracking experiments presented in the following sections were performed in these regions.

Organelles radius changed <20% within this z-range (Supplementary Fig. 1) showing that the error introduced in the radius determination is small when organelles are not completely in focus.

We also analyzed if there is a correlation between the size of melanosomes and their positions in the cell cytoplasm and could not detect a preferential distribution of different-sized organelles (Fig. 1E) suggesting that by sampling the different populations of organelles we are indeed sampling the whole cytoplasm.

3.2. Dynamics of organelles of different sizes in melanophore cells during aggregation

Melanophore cells were grown in coverslips, stimulated for aggregation as described in the Materials and methods section and observed using the brightfield microscope. We recorded image stacks of regions of the cells for 6 s using a frame time of 3 ms. This high data acquisition frequency allows extracting detailed information regarding the local dynamics of organelles in a temporal window that is significantly shorter than the whole aggregation process [14]. These movies were afterwards analyzed as described previously to obtain melanosome optical radii and trajectories (see Materials and methods).

Fig. 2A–B shows representative trajectories of a small and a big organelle (OR ~ 400 and 1100 nm, respectively) obtained with an accuracy of 4–7 nm using the pattern recognition algorithm. We observed that the trajectory of the small melanosome is more tortuous and less curvilinear compared to that of the big organelle. To quantify these qualitative observations, we calculated the mean square displacement (MSD, Eq. (1)) for each trajectory. This parameter indicates how far a particle traveled after a time lag τ and thus its dependence with τ is given by the motion properties of the particle and its microenvironment. Consequently, mechanisms underlying particle motion can be inferred from this analysis [27].

Fig. 2C shows that the MSD plots obtained for the trajectories observed in Fig. 2A–B followed an anomalous diffusion model (Eq. (2)) as was previously observed in many cellular systems. The anomalous diffusion exponent (α) constitutes a global parameter that indicates the overall directionality of the trajectory and is related to the balance of active vs. passive forces acting on the particle. In the absence of active processes such as those in ATP-depleted cells, the anomalous diffusion exponent (α) reflects the viscoelastic nature of the microenvironment and only subdifussion ($\alpha < 1$) is observed. In contrast, active forces driving organelles or endocytosed probes lead to superdiffusion [28] and it has been determined in a wide variety of systems that α values ranged 1.2–1.5 in these conditions [3,29–33].

Fig. 2D shows that the anomalous diffusion exponent increases as a function of the optical radius of melanosomes. While trajectories of small organelles present α values close to 1, which is the value expected for passive diffusion, big organelles showed α values of 1.3–1.4 indicating that these organelles are transported along more curvilinear pathways. Supplementary Fig. 2 shows additional examples of trajectories obtained for different sized melanosomes.

These results revealed that small organelles, which are supposed to experience a small drag force, present more tortuous trajectories. The rheological properties of the environment surrounding organelles influence their dynamics thus, we decided to explore the motility of melanosomes after depolymerizing different cytoskeleton networks in order to shed some light on the complex relationship shown in Fig. 2D. Particularly, we explore the influence of intermediate filaments in the observed behavior since as we mentioned above this intricate network seems to play a key role on melanosome transport. We also explored how the motility of big and small organelles is affected by actin since organelles may change their direction by switching between microtubules and actin filaments. To study if the observed behavior also depends on the stimulation condition of the cells, we performed these analyses in cells previously stimulated for aggregation or dispersion.

3.3. Depolymerization of actin filaments affects the mobility of small organelles during aggregation

We studied the dynamics of organelles in melanophore cells treated with latrunculin to depolymerize the actin filaments network;

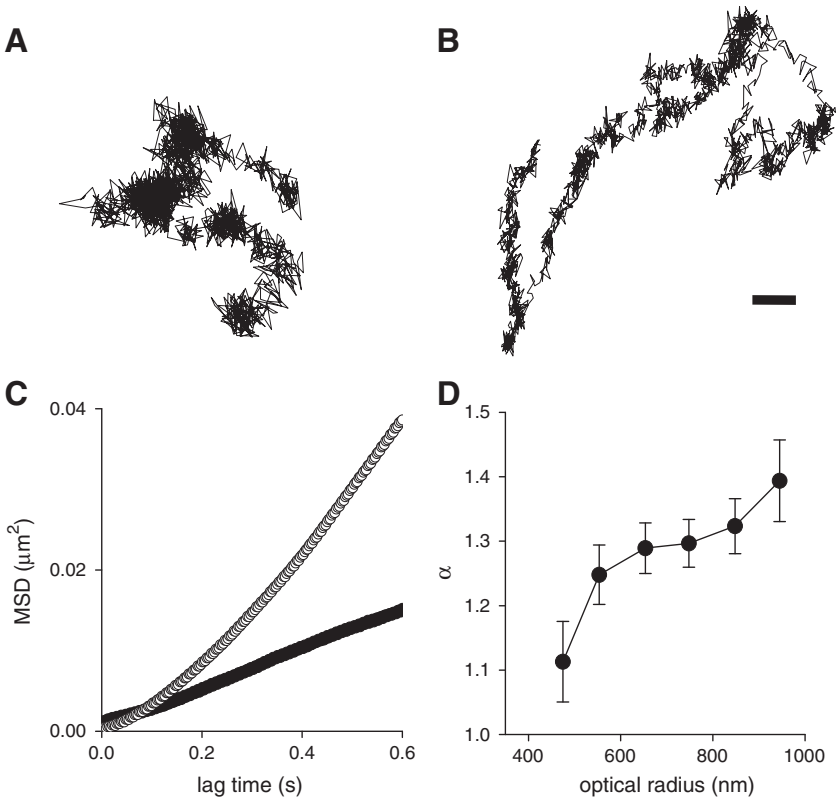

Fig. 2. Dependence of organelle dynamics on melanosome size during aggregation in wild type cells. Representative trajectories of melanosomes which optical radii were 430 nm (A) and 1160 nm (B). Scale bar, 100 nm. (C) These trajectories were analyzed as described in the text to obtain the mean square displacement for the small (●) and big (○) organelles. (D) Dependence of the anomalous diffusion coefficient (α) on melanosome optical radius. The MSD data obtained for each melanosome trajectory were fitted with Eq. (2) to determine the α value ($N = 300$). OR of these melanosomes were also measured as described in the text. The radii data were grouped in bins of 100 nm and the mean value of α obtained for each bin was plotted as a function of the mean radius in each interval. The error bars represents the standard error of the α determination in each bin.

in these conditions, transport only occurs along the microtubule network. We registered and analyzed trajectories of melanosomes during aggregation in latrunculin treated cells as described in the previous section. Fig. 3 shows that the anomalous diffusion exponent slightly increased with the melanosome optical radius reaching a value of ~1.3 which was not significantly different from the α value observed in Fig. 2D for big organelles. Interestingly, α values for melanosomes with radius < 700 nm were significantly higher than those observed in Fig. 2D (Supplementary Fig 3).

This result indicates that the myosin-actin transport system increases the tortuosity of trajectories of small organelles during aggregation but does not affect significantly the superdiffusive behavior of big organelles.

3.4. The intermediate filament network affects the dynamics of melanosomes

To study the influence of the intermediate filament network on melanosome motility we used a GFP-tagged dominant negative vimentin construct to disrupt the vimentin network (Fig. 4A–B, [11]) and studied melanosome dynamics as described in previous sections.

Fig. 4C shows that the motility of small organelles was markedly affected by the disruption of the vimentin network (Supplementary Fig. 4) while big melanosomes presented α values of ~1.3 suggesting that the native vimentin network increases the directionality of small organelles.

We have mentioned before that Chang et al. [11] showed that intermediate filaments constrain the motion of melanosomes; however the motility of the organelles was computed measuring the number of moving organelles and their velocities (calculated from the frame-to-frame displacement of the organelles, the frame rate in these experiments was 1 s). To compare our results obtained with millisecond resolution with those mentioned above, we used the same definition of velocity as in [11] and calculated the end-to-end velocity of melanosomes by measuring the distance traveled by the organelles after 1 s. With this definition, we also verified that the number of moving organelles was higher in the absence of an intermediate filament network (Supplementary Fig. 5). Taken together, these results suggest that vimentin filaments increase the directionality of small organelles but decrease the overall speed of the melanosomes.

We also assayed the dynamics of pigment organelles in vimentin dominant negative cells after depolymerizing the actin filament network with latrunculin (Fig. 4D). We verified that the anomalous diffusion exponent of small organelles in these treated cells is below 1 suggesting that these organelles are not actively transported. In contrast, the anomalous diffusion exponent of big organelles was not altered by the simultaneous depolymerization of vimentin and actin networks.

3.5. Dynamics of organelles during dispersion: contribution of the actin and intermediate filament networks

We studied the dynamics of melanosomes of different sizes in cells stimulated for dispersion as described in the Materials and methods section. With this aim, we registered images of regions of melanophore cells during the dispersion process and obtained melanosome trajectories and sizes by following the procedures described in the previous sections.

Fig. 5A shows the dependence of the anomalous diffusion exponent on melanosome OR for wild type conditions and for cells in which the actin and/or the intermediate filament networks were disrupted as described before. To make it easier for the comparison of results, we also included in the figure the data obtained for cells stimulated for aggregation (Fig. 5B). During dispersion, we verified that α increased with the organelles radius in most of the studied conditions. In addition, the anomalous diffusion exponent of both small and big organelles depended on the microenvironment (Supplementary Figs. 6–7) in contrast to the behavior observed during aggregation in which α for big organelles was ~1.3 in every assayed condition.

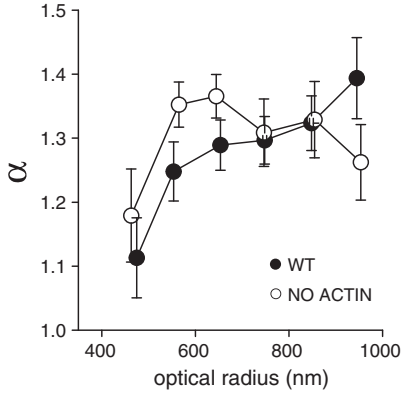

Fig. 3. Effects of actin filament network on melanosomes dynamics. Dependence of the anomalous diffusion exponent on melanosomes optical radius in actin-depolymerized cells (○). The number of trajectories analyzed was 300. To make the comparison of the data easier, the figure also includes the data presented in Fig. 2D (●).

Contrary to what was observed during melanosome aggregation, α values for wild type cells were significantly higher than those measured in cells in which the actin filament network was depolymerized. This result illustrates the different role of myosin-V dependent transport during aggregation and dispersion. As we mentioned in the Introduction, aggregation occurs predominantly along microtubules while dispersion involves both the microtubule and actin filaments networks (references in [34]). We will further discuss these differences below.

Disruption of the intermediate filaments network also reduced the directionality of melanosome trajectories during dispersion (i.e., α values were lower than those observed in WT cells). In addition, the anomalous diffusion exponents for small organelles were slightly but significantly higher than those measured during aggregation (Supplementary Fig. 8) suggesting that disruption of the IF network affects in a lower magnitude the active transport of small organelles during the dispersion process.

We also explored organelle dynamics in cells in which both the actin and IF networks were depolymerized and verified that there is no evident dependence of α on melanosome radius. In contrast to the behavior observed for aggregating cells in which small organelles were subdifussive (i.e. $\alpha \leq 1$) and big organelles presented α values of ~1.3, the anomalous diffusion exponent during dispersion was in the range 1.0–1.2.

4. Discussion

4.1. Influence of organelle size on melanosome transport during aggregation

In this work, we have studied the dynamics of organelles of different sizes in the cell cytoplasm with the aim of understanding the complex relation between organelle motion and microenvironment.

To measure the motion properties of organelles and other particles/molecules in living cells, different parameters such as run lengths [35], local and mean velocities [2,36] have been used before. The quantification of these parameters usually requires applying arbitrary criteria for selecting specific regions of the trajectories with certain properties and thus relevant information may be lost in this analysis. In our study, we used the anomalous diffusion exponent as an indicator of mobility since this exponent gives valuable information regarding the topography of the whole trajectories and thus of the processes causing it. While particles moving following pure motion mechanisms such as random diffusion and active transport along linear paths present trajectories that are characterized by α values of 1 and 2, respectively, motion of organelles in the cell cytoplasm cannot be represented by such simple models. In fact, organelle dynamics includes periods of active transport, switches of directions and periods in which the organelles move

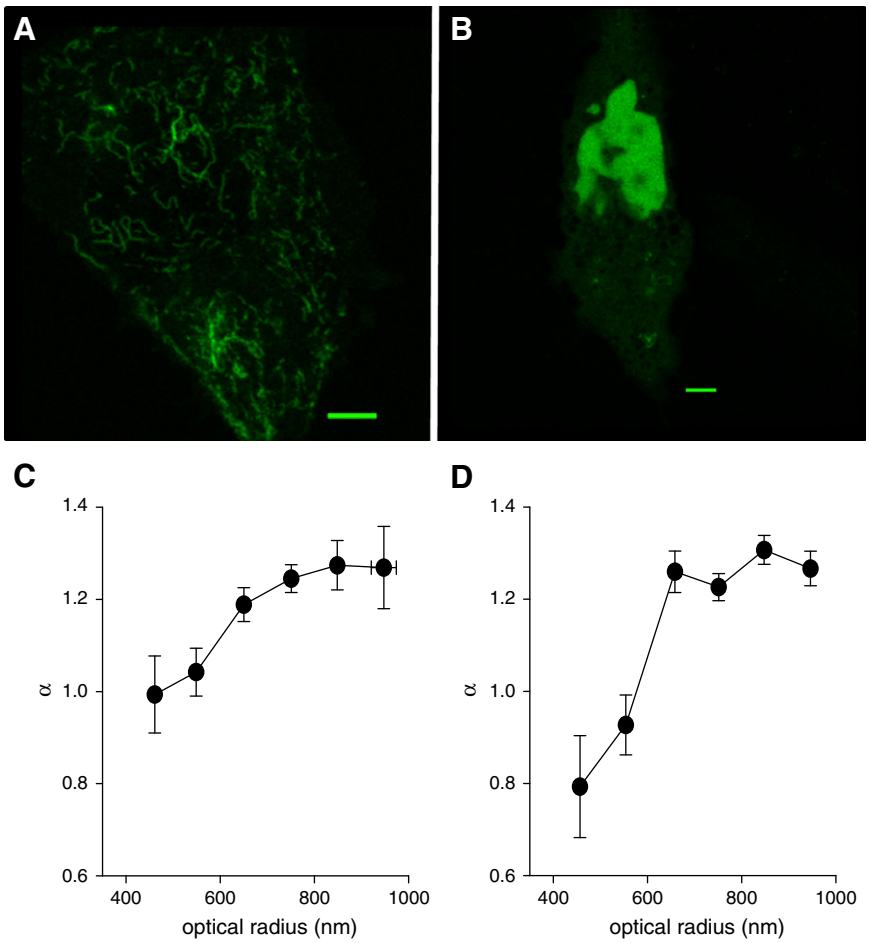

Fig. 4. Role of vimentin intermediate filament network on organelles dynamics. Confocal images of melanophore cells transfected as described in the text with GFP-vimentin (A) and GFP-tagged dominant negative construct (B). Scale bar, 5 μm. Trajectories and radii of melanosomes were registered in melanophores cells in which either the vimentin filament network (C) or the actin and the vimentin filament networks (D) were disrupted. The anomalous diffusion exponent was determined for each trajectory and plotted as a function of melanosome optical radius as described in the legend to Fig. 2. The number of trajectories analyzed was 285 and 428 (C and D, respectively).

passively or is indirectly pushed by other forces such as those involved in the continuous reorganization of the cytoskeleton.

Melanosome transport is a relatively well studied process (reviewed in [14,37]). It has been proposed that microtubule motors are responsible for the long-distance transport of organelles and the actin-dependent motor myosin V is associated to short-distance movements [38]. While pigment aggregation occurs predominantly along microtubules driven by cytoplasmic dynein, pigment dispersion involves both, the microtubule motor kinesin-2 and the actin-dependent motor myosin-V (references in [34]). Since dynamics of melanosomes included the action of 3 different types of motors moving along 2 different types of tracks we simplified the system and studied the dynamics of the organelles in cells in which different components of the cytoskeleton were depolymerized.

Initially, we studied the dynamics of melanosomes in cells stimulated for aggregation. Our results showed that the anomalous diffusion exponent increases with organelle size reaching a constant value of ~1.3 in every assayed condition, these values are in agreement with those reported for engulfed microbeads and organelles in living cells [3,29–33].

Interestingly, we also observed that the value of α for big organelles did not depend on the presence of either actin or intermediate filaments suggesting that the tortuosity of the trajectories of big organelles is defined mostly by the properties of microtubule-dependent transport. In contrast, the anomalous diffusion exponent of small organelles increases with size in most of the assayed conditions and was very sensitive to the presence of either actin or intermediate filaments. These results suggest that small organelles may switch tracks/direction more frequently than big organelles and/or present a higher detachment probability from the cytoskeleton track.

Considering that big organelles are more processive than small organelles and processivity increases with the number of motors actively pulling the organelle [39–42] we propose that big organelles are transported by a higher number of active motor molecules. According to this hypothesis (schematized in Fig. 6), the collective transport of big organelles will probably introduce a lower number of reversions and switches to other microtubules or actin filaments [43,44]. Importantly, we do not consider that transport of organelles is driven by a single team of identical microtubule motors. In fact, it is now well accepted that transport of organelles along microtubules involves a stochastic tug-of-war between teams of opposed-polarity motors, the team that exerts more force on the cargo at a given moment determine the direction of transport (see for example, [45,46]). Moreover, Muller et al. [40] recently showed theoretically that cargo processivity is strongly enhanced by transport via several molecular motors even if these motors are engaged in a tug-of-war.

We also explored the influence of actin filaments on melanosome transport during aggregation and verified that depolymerization of these filaments decreased the tortuosity of small melanosome trajectories and caused no effect on the trajectories of big organelles (Fig. 3). Considering that myosin V competes with microtubule motors through a tug-of-war mechanism [21], our model predicts that

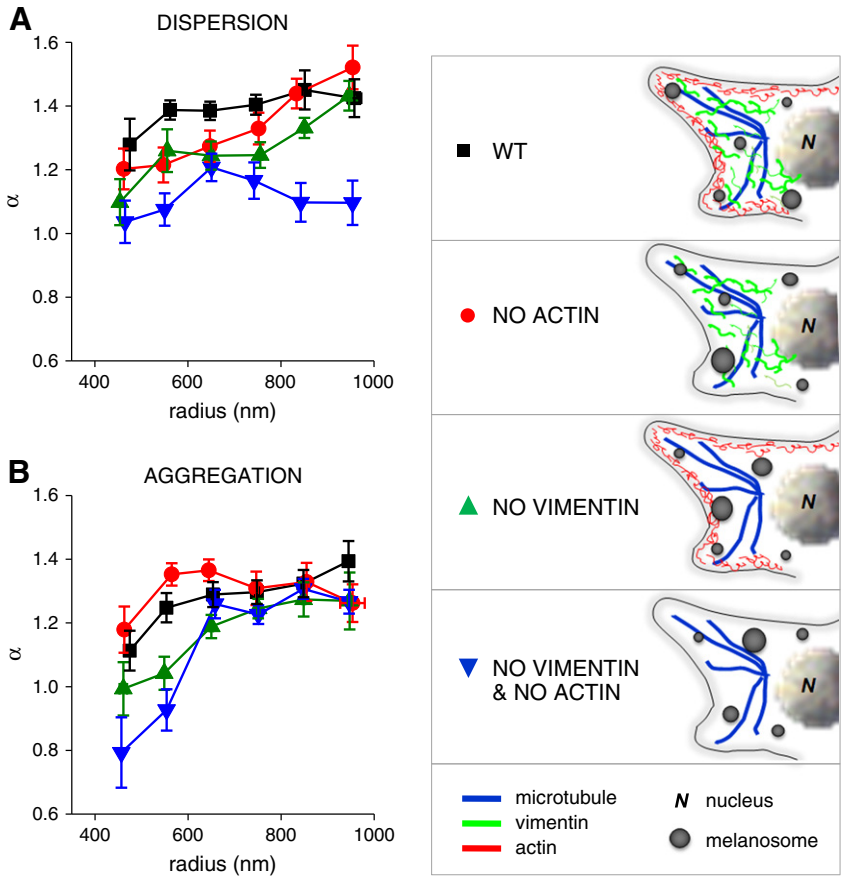

Fig. 5. Dependence of organelle dynamics on melanosome size in cells stimulated for dispersion. Trajectories (N ~ 300 for each condition) and radii of melanosomes were registered in melanophores wild type cells (■, black) or in cells treated to disrupt actin filaments (●, red), vimentin intermediate filaments (▲, green) or vimentin and actin filament networks (▼, blue). The anomalous diffusion coefficient was determined for each trajectory and plotted as a function of melanosome OR as described in the legend to Fig. 2. To make it easier the comparison of data, the figure also includes the results obtained during the aggregation process (B).

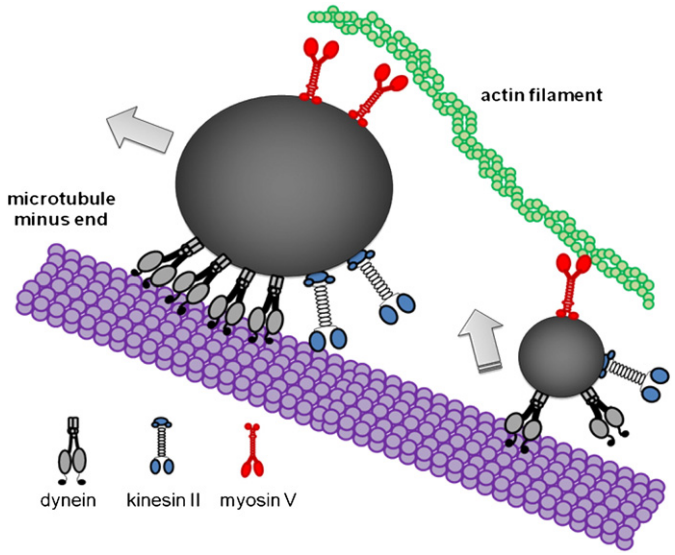

Fig. 6. Schematic representation of the influence of organelle size on transport during aggregation. A big organelle attached to a higher number of microtubule and actin-dependent motors is represented in this cartoon; the organelle moves by the action of several copies of dynein motors that move processively toward the minus end of the microtubule. These motors "win" the tug of war against myosin V and kinesin-2 as previously proposed. The small organelle represented in the figure is driven by a single dynein motor and thus the probability of detaching from the track and/or switching directions increases. The intermediate filament network (not represented) constrains the motion of organelles increasing the probability of reattachment.

switches from microtubules to actin filaments will be less frequent for big than for small organelles because the latter are attached to a lower number of active microtubule motors. Consequently, the tortuosity of trajectories of small organelles will be higher in the presence of actin. Actin filaments may also constitute passive obstacles to the transport since run lengths of melanosomes along microtubules increases after depolymerization of actin filaments [35]. Thus small organelles – which have a lower number of motor copies – may detach easier than big organelles in the presence of these obstacles.

Surprisingly, we found that the anomalous diffusion exponent of small organelles significantly decreases after depolymerization of intermediate filaments either in the presence or absence of actin filaments. Moreover, in the absence of actin and intermediate filaments, α values were smaller than 1 suggesting that these organelles are not actively transported.

These results could be interpreted considering that vimentin filaments may acts as a physical network that maintains organelles close to microtubules or actin filaments allowing the efficient reattachment of free organelles to the track. This model is similar to that proposed by Potokar et al. [13] to explain the role of intermediate filaments in transport of vesicles in astrocytes. In the same direction, Hendricks et al. [47] has recently proposed that the viscoelastic microenvironment confines diffusion, increasing the time that cargoes remain near the microtubule, thus promoting motor binding.

According to our model, the transport of small organelles – that detach from the track more frequently than big organelles – is very sensitive to the presence of the stabilizing intermediate filament network. In contrast, the intermediate filament network does not play a significant role in the transport of big organelles suggesting that the

presence of multiple copies of active motors guarantee a low detachment probability.

Previous works demonstrated that vimentin disruption enhances melanosome motility and mean velocity [11]. These results seem to be in contradiction with those showed in our work however, our study was performed with millisecond temporal resolution and in a significantly shorter temporal window; therefore we analyzed the fast, local dynamics of organelles while Chang et al. [11] measured the overall dynamics in the second time-scale. After resampling our data with the temporal resolution used by Chang et al. [11] and interpret these data with the mobility parameters used in that work, the results obtained are comparable to those previously reported (Supplementary Fig. 5).

4.2. Influence of organelle size on melanosome transport during dispersion

We also verified that the anomalous diffusion exponent depends on the melanosome radius in cells stimulated for dispersion but the behavior seemed different to that observed for aggregating cells.

Particularly, we verified that actin increased the directionality of organelles during dispersion and has the opposed effect during aggregation since α values for small organelles in actin depleted cells were lower than that observed in wild type cells during dispersion in opposition to the behavior observed in aggregation (Fig. 5).

These results show that both actin and microtubule transports contribute to the overall organelle dynamics during the dispersion process in contrast to aggregation in which the behavior of the organelles seems to be governed by dynein motors. Importantly, several works have also showed the relevance of actin-dependent transport to the dispersion process. Specifically, it has been demonstrated that melanosomes have a higher number of copies of myosin V attached to them after stimulating the cells for dispersion [21] and as a consequence, move longer distances without detaching from the track [3] or switching directions [48]. Also, Slepcheko et al. [34] suggested that the transfer rate of melanosomes from actin filaments to microtubules is lower in dispersing than in aggregating cells. More recently, Schroeder et al. [43,44] measured the switching probability between microtubules and actin filaments of beads transported by microtubule and actin motors and concluded that the dissociation kinetics of kinesin-2 favor switching from microtubules to actin filaments, consistent with transport during dispersion.

The intricate intermediate filament network also affected microtubule-dependent transport during dispersion. Surprisingly, small organelles in the absence of IF and actin presented α values of 1–1.2 in dispersing cells while these organelles were subdifussive during aggregation. These results can be explained considering the better performance of kinesin-2 vs. dynein at a single molecule level [41,44,49]. Interestingly, α values measured in the absence of IF and actin did not depend on the organelle size suggesting that both small and big organelles have a similar detachment probability. This result suggests that kinesin-driven transport requires a lower number of copies of the active motor in comparison to dynein-dependent transport agreeing with previous studies that showed that bidirectional cargoes are often driven by a single kinesin motor and many weak dynein motors [46].

Importantly, we observed a dependence of α on organelle size in cells in which only intermediate filaments were depolymerized. In these cells, transport is driven by both microtubule and actin dependent motors. Previously, we mentioned that the anomalous diffusion exponent of kinesin-driven transport in the absence of IF did not depend on organelle size. Thus, these results suggest that organelle size may also influence actin dependent transport.

In conclusion, in this work we verified that the size of organelles influence their dynamics in unexpected ways. While the drag force exerted by the medium is supposed to increase with the size of the cargo, we found that small organelles are more sensitive to the properties of their microenvironment than big organelles and that this behavior is probably tuned by the number of active motors effectively pulling the organelle.

Acknowledgments

We are grateful to Martín Dodes Traian for kindly helping us with C-laurdan imaging and Lorena Benseñor for helpful discussion. This research was supported by ANPCyT (PICT 2008-1104) and UBACyT (20020110100074). LB, MAD, AW and VL are members of CONICET.

Appendix A. Supplementary data

Supplementary data to this article can be found online at http://dx.doi.org/10.1016/j.bbagen.2013.06.043.

References

[1] Y. Ishii, T. Yanagida, Single molecule measurments and molecular motors, in: M. Schliwa (Ed.), Molecular Motors, Wiley-VCH, Munchen, 2003.
[2] V. Levi, A.S. Serpinskaya, E. Gratton, V. Gelfand, Organelle transport along microtubules in *Xenopus* melanophores: evidence for cooperation between multiple motors, Biophys. J. 90 (2006) 318–327.
[3] M. Brunstein, L. Bruno, M. Desposito, V. Levi, Anomalous dynamics of melanosomes driven by myosin-V in *Xenopus laevis* melanophores, Biophys. J. 97 (2009) 1548–1557.
[4] L. Bruno, M.M. Echarte, V. Levi, Exchange of microtubule molecular motors during melanosome transport in *Xenopus laevis* melanophores is triggered by collisions with intracellular obstacles, Cell Biochem. Biophys. 52 (2008) 191–201.
[5] V. Levi, V.I. Gelfand, A.S. Serpinskaya, E. Gratton, Melanosomes transported by myosin-V in *Xenopus* melanophores perform slow 35 nm steps, Biophys. J. 90 (2006) L7–L9.
[6] R. Mallik, S.P. Gross, Molecular motors: strategies to get along, Curr. Biol. 14 (2004) R971–R982.
[7] R.D. Vale, The molecular motor toolbox for intracellular transport, Cell 112 (2003) 467–480.
[8] I.M. Kulic, A.E.X. Brown, H. Kim, C. Kural, B. Blehm, P.R. Selvin, P.C. Nelson, V. Gelfand, The role of microtubule movement in bidirectional organelle transport, Proc. Natl. Acad. Sci. U. S. A. 105 (2008) 10011–10016.
[9] I. Semenova, A. Buralov, N. Berardone, I. Zaliapin, B. Slepchenko, T. Svittkina, A. Kashina, V. Rodionov, Actin dynamics is essential for myosin-based transport of membrane organelles, Curr. Biol. 18 (2008) 1581–1586.
[10] C. Kural, A.S. Serpinskaya, Y. Chou, R.D. Goldman, V.I. Gelfand, P.R. Selvin, Tracking melanosomes inside a cell to study molecular motors and their interaction, Proc. Natl. Acad. Sci. U. S. A. 104 (2007) 5378–5382.
[11] L. Chang, K. Barlan, Y.H. Chou, B. Grin, M. Lakonishok, A.S. Serpinskaya, D.K. Shumaker, H. Herrmann, V.I. Gelfand, R.D. Goldman, The dynamic properties of intermediate filaments during organelle transport, J. Cell Sci. 122 (2009) 2914–2923.
[12] O.E. Nekrasova, M.G. Mendez, I.S. Chernoivanenko, P.A. Tyurin-Kuzmin, E.R. Kuczmarski, V.I. Gelfand, R.D. Goldman, A.A. Minin, Vimentin intermediate filaments modulate the motility of mitochondria, Mol. Biol. Cell 22 (2011) 2282–2289.
[13] M. Potokar, M. Kreft, L. Li, J. Daniel Andersson, T. Pangrsic, H.H. Chowdhury, M. Pekny, R. Zorec, Cytoskeleton and vesicle mobility in astrocytes, Traffic 8 (2007) 12–20.
[14] A.A. Nascimento, J.T. Roland, V.I. Gelfand, Pigment cells: a model for the study of organelle transport, Annu. Rev. Cell Dev. Biol. 19 (2003) 469–491.
[15] M.M. Rozdzial, L.T. Haimo, Bidirectional pigment granule movements of melanophores are regulated by protein phosphorylation and dephosphorylation, Cell 47 (1986) 1061–1070.
[16] P.J. Sammak, S.R. Adams, A.T. Harootunian, M. Schliwa, R.Y. Tsien, Intracellular cyclic AMP not calcium, determines the direction of vesicle movement in melanophores: direct measurement by fluorescence ratio imaging, J. Cell Biol. 117 (1992) 57–72.
[17] H. Nilsson, M. Wallin, Evidence for several roles of dynein in pigment transport in melanophores, Cell Motil. Cytoskeleton 38 (1997) 397–409.
[18] M.C. Tuma, A. Zill, N. Le Bot, I. Vernos, V. Gelfand, Heterotrimeric kinesin II is the microtubule motor protein responsible for pigment dispersion in *Xenopus* melanophores, J. Cell Biol. 143 (1998) 1547–1558.
[19] S.L. Rogers, R.L. Karcher, J.T. Roland, A.A. Minin, S.W.V.I. Gelfand, Regulation of melanosome movement in the cell cycle by reversible association with myosin V, J. Cell Sci. 146 (1999) 1265–1276.
[20] S.L. Rogers, I.S. Tint, P.C. Fanapour, V.I. Gelfand, Regulated bidirectional motility of melanophore pigment granules along microtubules in vitro, Proc. Natl. Acad. Sci. U. S. A. 94 (1997) 3720–3725.
[21] S.P. Gross, M.C. Tuma, S.W. Deacon, A.S. Serpinskaya, A.R. Reilein, V.I. Gelfand, Interactions and regulation of molecular motors in *Xenopus* melanophores, J. Cell Biol. 156 (2002) 855–865.
[22] S.L. Rogers, I.S. Tint, V.I. Gelfand, In vitro motility assay for melanophore pigment organelles, Methods Enzymol. 298 (1998) 361–372.

[23] J. Turkevich, P. Cooper Stevenson, J. Hillier, A study of the nucleation and growth processes in the synthesis of colloidal gold, Discuss. Faraday Soc. 11 (1951) 55–75.
[24] M.M. Dodes Traian, F.L. Gonzalez Flecha, V. Levi, Imaging lipid lateral organization in membranes with C-laurdan in a confocal microscope, J. Lipid Res. 53 (2012) 609–616.
[25] M.J. Saxton, K. Jacobson, Single-particle tracking: applications to membrane dynamics, Annu. Rev. Biophys. Biomol. Struct. 26 (1997) 373–399.
[26] R. Wayne, Light and Video Microscopy, Elsevier Inc., Amsterdam, 2009. 35–65.
[27] V. Levi, E. Gratton, Exploring dynamics in living cells by tracking single particles, Cell Biochem. Biophys. 48 (2007) 1–15.
[28] D. Robert, K. Aubertin, J.C. Bacri, C. Wilhelm, Magnetic nanomanipulations inside living cells compared with passive tracking of nanoprobes to get consensus for intracellular mechanics, Phys. Rev. E Stat. Nonlinear Soft Matter Phys. 85 (2012) 011905.
[29] L. Bruno, V. Levi, M. Brunstein, M.A. Desposito, Transition to superdiffusive behavior in intracellular actin-based transport mediated by molecular motors, Phys. Rev. E Stat. Nonlinear Soft Matter Phys. 80 (2009) 011912.
[30] H. Salman, Y. Gil, R. Granek, M. Elbaum, Microtubules, motor proteins, and anomalous mean squared displacements, Chem. Phys. 284 (2002) 389–397.
[31] A. Caspi, R. Granek, M. Elbaum, Diffusion and directed motion in cellular transport, Phys. Rev. E Stat. Nonlinear Soft Matter Phys. 66 (2002) 011916.
[32] N. Gal, D. Weihs, Experimental evidence of strong anomalous diffusion in living cells, Phys. Rev. E Stat. Nonlinear Soft Matter Phys. 81 (2010) 020903.
[33] C. Wilhelm, Out-of-equilibrium microrheology inside living cells, Phys. Rev. Lett. 101 (2008) 028101.
[34] B.M. Slepchenko, I. Semenova, I. Zaliapin, V. Rodionov, Switching of membrane organelles between cytoskeletal transport systems is determined by regulation of the microtubule-based transport, J. Cell Biol. 179 (2007) 635–641.
[35] S.P. Gross, M.A. Welte, S.M. Block, E.F. Wieschaus, Dynein-mediated cargo transport in vivo. A switch controls travel distance, J. Cell Biol. 148 (2000) 945–956.
[36] A. Snezhko, K. Barlan, I.S. Aranson, V.I. Gelfand, Statistics of active transport in *Xenopus* melanophores cells, Biophys. J. 99 (2010) 3216–3223.
[37] S. Aspengren, New insights into melanosome transport in vertebrate pigment cells, Int. J. Cell Mol. Biol. 272 (2009) 245–302.
[38] G.M. Langford, Actin- and microtubule-dependent organelle motors: interrelationships between the two motility systems, Curr. Opin. Cell Biol. 7 (1995) 82–88.
[39] J. Beeg, S. Klumpp, R. Dimova, R.S. Gracia, E. Unger, R. Lipowsky, Transport of beads by several kinesin motors, Biophys. J. 94 (2008) 532–541.
[40] M.J. Muller, S. Klumpp, R. Lipowsky, Bidirectional transport by molecular motors: enhanced processivity and response to external forces, Biophys. J. 98 (2010) 2610–2618.
[41] R. Mallik, D. Petrov, S.A. Lex, S.J. King, S.P. Gross, Building complexity: an in vitro study of cytoplasmic dynein with in vivo implications, Curr. Biol. 15 (2005) 2075–2085.
[42] M. Vershinin, B.C. Carter, D.S. Razafsky, S.J. King, S.P. Gross, Multiple-motor based transport and its regulation by tau, Proc. Natl. Acad. Sci. U. S. A. 104 (2007) 87–92.
[43] H.W. Schroeder III, C. Mitchell, H. Shuman, E.L. Holzbaur, Y.E. Goldman, Motor number controls cargo switching at actin-microtubule intersections in vitro, Curr. Biol. 20 (2010) 687–696.
[44] H.W. Schroeder III, A.G. Hendricks, K. Ikeda, H. Shuman, V. Rodionov, M. Ikebe, Y.E. Goldman, E.L. Holzbaur, Force-dependent detachment of kinesin-2 biases track switching at cytoskeletal filament intersections, Biophys. J. 103 (2012) 48–58.
[45] A.G. Hendricks, E. Perlson, J.L. Ross, H.W. Schroeder III, M. Tokito, E.L. Holzbaur, Motor coordination via a tug-of-war mechanism drives bidirectional vesicle transport, Curr. Biol. 20 (2010) 697–702.
[46] V. Soppina, A.K. Rai, A.J. Ramaiya, P. Barak, R. Mallik, Tug-of-war between dissimilar teams of microtubule motors regulates transport and fission of endosomes, Proc. Natl. Acad. Sci. U. S. A. 106 (2009) 19381–19386.
[47] A.G. Hendricks, E.L. Holzbaur, Y.E. Goldman, Force measurements on cargoes in living cells reveal collective dynamics of microtubule motors, Proc. Natl. Acad. Sci. U. S. A. 109 (2012) 18447–18452.
[48] J. Snider, F. Lin, N. Zahedi, V. Rodionov, C.C. Yu, S.P. Gross, Intracellular actin-based transport: how far you go depends on how often you switch, Proc. Natl. Acad. Sci. U. S. A. 101 (2004) 13204–13209.
[49] G. Muthukrishnan, Y. Zhang, S. Shastry, W.O. Hancock, The processivity of kinesin-2 motors suggests diminished front-head gating, Curr. Biol. 19 (2009) 442–447.